ACS APPLIED MATERIALS & INTERFACES

Research Article

www.acsami.org

Intracellular Antioxidants Dissolve Man-Made Antioxidant Nanoparticles: Using Redox Vulnerability of Nanoceria to Develop a Responsive Drug Delivery System

Faheem Muhammad,[†,‡] Aifei Wang,[†] Wenxiu Qi,[‡] Shixing Zhang,[†] and Guangshan Zhu*[,†]

[†]State Key Laboratory of Inorganic Synthesis and Preparative Chemistry, College of Chemistry, [‡]College of Life Science, Jilin University, Changchun 130012, P. R. China

Supporting Information

ABSTRACT: Regeneratable antioxidant property of nanoceria has widely been explored to minimize the deleterious influences of reactive oxygen species. Limited information is, however, available regarding the biological interactions and subsequent fate of nanoceria in body fluids. This study demonstrates a surprising dissolution of stable and ultrasmall (4 nm) cerium oxide nanoparticles (CeO_2 NPs) in response to biologically prevalent antioxidant molecules (glutathione, vitamin C). Such a redox sensitive behavior of CeO_2 NPs is subsequently exploited to design a redox responsive drug delivery system for transporting anticancer drug (camptothecin). Upon exposing the CeO_2 capped and drug loaded nanoconstruct to vitamin c or glutathione, dissolution-accompanied aggregation of CeO_2 nanolids unleashes the drug molecules from porous silica to achieve a significant anticancer activity. Besides stimuli responsive drug delivery, immobilization of nanoceria onto the surface of mesoporous silica also facilitates us to gain a basic insight into the biotransformation of CeO_2 in physiological mediums.

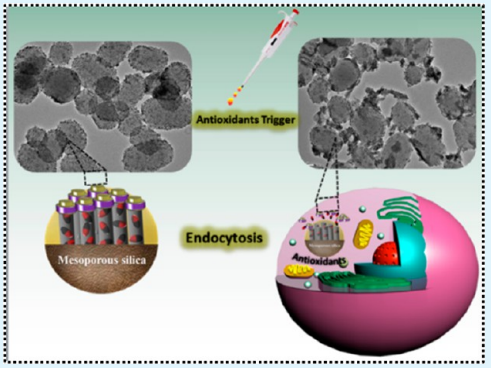

KEYWORDS: *nanoceria, antioxidants, reactive oxygen species, controlled release, redox responsive, chemotherapy*

1. INTRODUCTION

Oxidative stress is considered a major culprit in triggering a large number of devastating diseases, such as cancer, aging processes, neurodegenerative, and vascular disorders.[1−3] Normally, cells produce number of enzymatic and nonenzymatic chemicals to defend themselves against oxidative stress.[4−6] Superoxide dismutase and catalase are two prominent antioxidant enzymes which serve as scavengers against major intracellular reactive oxygen species (ROS), such as superoxide and hydrogen peroxide, to minimize bimolecular damage. Besides biological enzymes, the recent boom in nanotechnology has fortunately provided us number of other nanoparticle based alternatives.[7−10] For instance, exceptional antioxidant properties of cerium oxide nanoparticles (CeO_2 NPs) have recently spurred a great deal of research interest for potentially treating various oxidative-stress related complications. Over the past decade, we have witnessed extensive biological studies, which established CeO_2 neuroprotective, anti-inflammatory, antiaging, and cardioprotective potentials.[11−16] Therapeutic attributes of highly biocompatible CeO_2 NPs are ascribed to its excellent ability to detoxify superoxide and hydrogen peroxide species, thus mimicking the role of superoxide dismutase and catalase.[17,18] In chemical terms, the reversible switching of oxidation states (+3 and +4) is responsible for the unique therapeutic activity of CeO_2 NPs.[19,20] Two main factors influence its efficacy; particle size is the first determinant, which accounts for the antioxidant property. Ultrasmall CeO_2 NPs have been proven more potent antioxidants due to the presence of higher surface to volume ratio for better oxygen exchange and redox reactions; second, the existence of trivalent cerium (Ce^{3+}) is essential for its biocatalytic activity which increases with decreasing particle size.

In case of ROS exposure, Ce^{3+} is oxidized into Ce^{4+} and surprisingly over the passage of time the oxidized Ce^{4+} reverts back to its original state. Such autoregeneration is a unique characteristic of CeO_2 NPs, whereas other antioxidant nanoparticles such as hydroxylated SWCNTs and C-60 are irreversibly degenerated such as biological molecules.[21] Besides these therapeutic attributes, nanoceria is also one of the 13 intensively used nanomaterials and being consumed in a wide range of applications including catalysis, additive in fuel, automotive catalytic converters, oxygen sensors, solid oxide fuel cells, UV absorbers, and glass polishing. Due to growing use of CeO_2 NPs, its contact with living organism is now inevitable; therefore, there is a great deal of concern to evaluate its potential impacts on biotic world. Nanoceria is mostly found passive in nature and remains in a nanoparticulate form for long period of time and cell viability data also demonstrates its biocompatibility and low or no toxicity.[22,23] To this end, few reports investigated

Received: August 17, 2014
Accepted: October 14, 2014
Published: October 14, 2014

Scheme 1. Schematic Demonstration of Synthetic and Working Protocol for Antioxidant Responsive Drug Delivery System

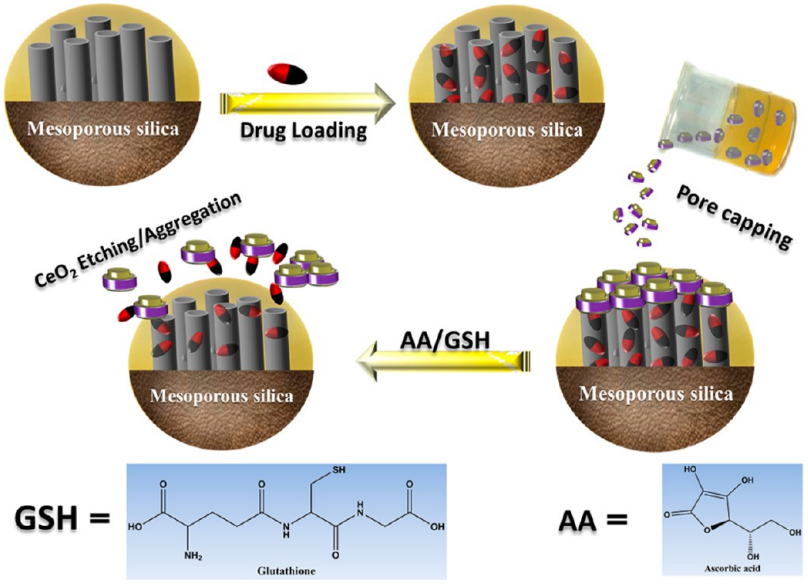

the interaction of nanoceria in different animal and plants models. For instance, Zhang et al. studied the effect of CeO_2 NPs in cucumber plant, their results demonstrated that the most of the adsorbed NPs were bioretained, however; a small fraction was biotransformed into $CePO_4$ in roots and cerium carboxylates in shoots.[24] Other efforts also corroborated the stability of nanoceria with a slight dissolution in environmental media and plants. Cornelis et al. found a slight dissolution (<3.1%) of nanoceria in soil solution at pH 4, but no decomposition was noticed at pH 7 and 9.[25] Moreover, both in vitro and in vivo animal studies were also conducted, using various sizes of nanoceria, to assess the cytotoxicity.[26] Sanjay and co-workers recently explored the effect of phosphate group on the antioxidant activity of CeO_2.[27] Despite these preliminary developments, the massive use of CeO_2 nanoparticles demands, as evidenced by the OECD list, which put nanoceria on priority for immediate testing, a comprehensive evaluation of its biotransformation, fate, and subsequent toxicity. In this study, we investigated the interaction of high quality antioxidant nanoparticles (CeO_2) with biologically prevalent antioxidant molecules (vitamin C and glutathione). Surprisingly, stabilized CeO_2 NPs were etched upon exposing to biorelavent antioxidants. Based on these findings, we decided to use this biological interaction as lucrative target for therapeutic advantages. Over the years, tremendous research activity has been witnessed in nanomedicine to develop stimuli-responsive nanocarriers for specifically targeting the diseased area via using pathophysiological signals of diseases.[28−33] In this regard, mesoporous silica nanoparticles (MSNs) have emerged as ideal drug nanocarriers to develop various stimuli responsive drug delivery systems due to its excellent stability, versatile nano-architecture, and availability of both inner nanochannels and outer surface area to manipulate the release behavior of loaded guest molecules.[34,35] Several environmental triggers, namely, pH, disulfide cleaving reducing agents, temperature, light, magnetic field, electric field, glucose, enzymes, and ultrasound, etc., have until now been explored.[36−40]

Despite significant progress in stimuli responsive nanosystems as a new therapeutic tactic, research community is still in search of new and multipurpose nanocarriers, which specifically respond to biologically prevalent signals and accordingly deliver therapeutics in a spatially and temporally sustained fashion. In this contribution, we report on the fabrication of antioxidant responsive drug delivery system, based on the redox susceptibility of nanoceria to biologically prevalent reducing agents. When drug loaded and ceria capped nanoparticles are exposed to vitamin C or glutathione, CeO_2 are rapidly etched, which in turns open the nanochannels of MSNs to permit controlled release of anticancer drug. Scheme 1 illustrates the synthetic and working protocol for antioxidant responsive drug delivery system.

2. RESULTS AND DISSCUSSION

Rather than preparing hydrophobic CeO_2 NPs by using high temperature and organic surfactants,[9,41] we have followed a straightforward and reproducible strategy to prepare water based nanoceria at quite low temperature (65 °C), without using any surfactant molecules.[42] However, the method that we have followed produced an aggregated product, which cannot be further used as nanolids to block the nanochannels of MSNs. To address this issue, one additional step was carried out in which the surface of aggregated CeO_2 NPs was stabilized with citric acid. Citric acid is a strong and widely used chelating agent, which predominantly chemisorbs onto the surface of metal nanoparticles through establishing a carboxylate complex with metals surface, as confirmed by IR analysis (Supporting Information Figure S2). After citric acid conjugation, the colloidal stability was markedly improved; photographs of both samples before and after CA stabilizations displayed a radical difference between the turbidity of solutions (inset of Figure 3b). We also measured the ζ-potential of CeO_2 NPs and CeO_2-CA NPs to determine the surface modification. Supporting Information Table S1 illustrates that the positive ζ-potential value of CeO_2 NPs (35.5 mV) is significantly changed to a negative one (−34.4 mV), which suggests the successful conjugation of citrate groups onto the surface of CeO_2 NPs. Due to significant citric acid conjugation, a highly concentrated solution of water stable and ultrasmall CeO_2 was obtained, whose strength was found to be as high as 60 g/L (~350 mmol/L). The transparency of concentrated solution depicts the quality of product, which was extremely desirable for gatekeeping protocol of MSNs.

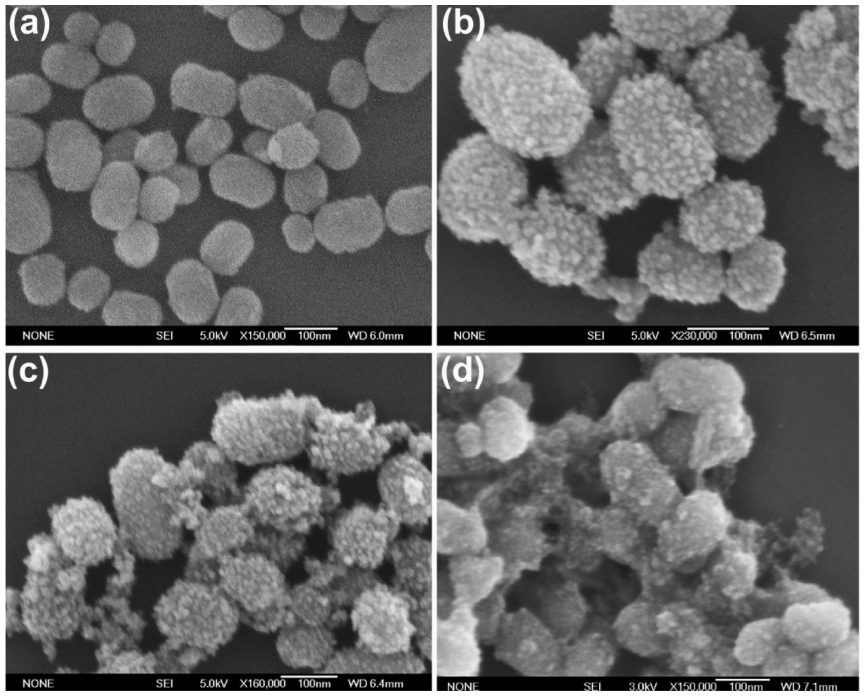

Figure 1. (a) SEM micrograph of MSNs-NH_2. (b) CeO_2 capped MSNs. (c) Image is obtained after treating CeO_2@MSNs with 2 mM vitamin C. (d) CeO_2 capped MSNs sample after 2 mM glutathione exposure.

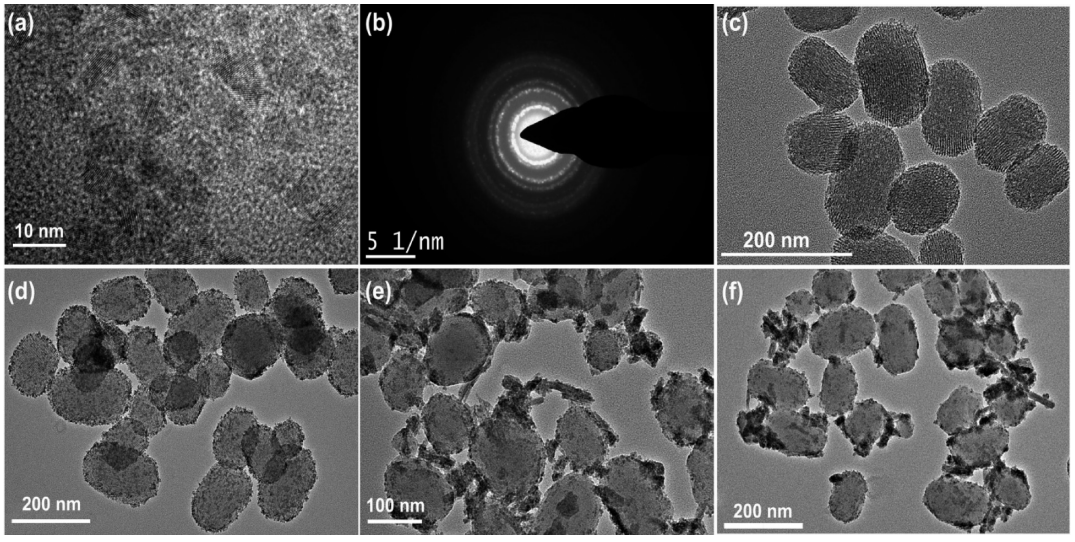

Figure 2. (a) HR-TEM image of citrate stabilized CeO_2 NPs. (b) Selected area electron diffraction (SAED) patterns of CeO_2 NPs. (c) TEM micrograph of MSNs-NH2. (d) CeO_2 capped MSNs nanocomposite. (e) TEM obtained after treating CeO_2@MSNs with 2 mM vitamin C. (f) CeO_2 capped MSNs sample after 2 mM glutathione exposure.

Ultrasmall CeO_2 NPs hydrosol was subsequently characterized using both analytical and spectroscopic techniques. TEM examination reveals roughly spherical and well dispersed CeO_2 product with an average diameter of 4 ± 1 nm, it should be kept in mind that synthesis of ultrasmall and uniform nanoparticles is highly sought-after to achieve excellent antioxidant properties as well. Figure 2a displays the corresponding HR-TEM image, which indicates a monocrystalline nature of citric acid functionalized CeO_2 NPs. Selected area electron diffraction (SAED) patterns indicated a cubic fluorite structure of CeO_2 NPs (Figure 2b). The purity and crystallinity of CeO_2 NPs was identified through analyzing the XRD patterns of powdered samples. XRD patterns of the nanoparticles (Figure 3a) demonstrated a cubic phase of CeO_2 (JCPDS card number 34-0394), while broadness of corresponding diffraction peaks suggested the formation of ultrasmall ceria nanoparticles.

Furthermore, the composition and surface modifications of CeO_2 NPs were determined through X-ray photoelectron spectroscopy (XPS) and Fourier transform infrared spectroscopy (FTIR). Supporting Information Figure S3 displays the survey spectrum of samples, which shows the presence of Ce, O, and C as the primary components. High resolution XPS spectrum manifested mixed oxidation states (Ce^{3+} and Ce^{4+}), coexistence of mixed valence states is vital for optical and antioxidant attributes of CeO_2 NPs and the same mixed oxidation states works for CeO_2 dissolution phenomenon in current study.

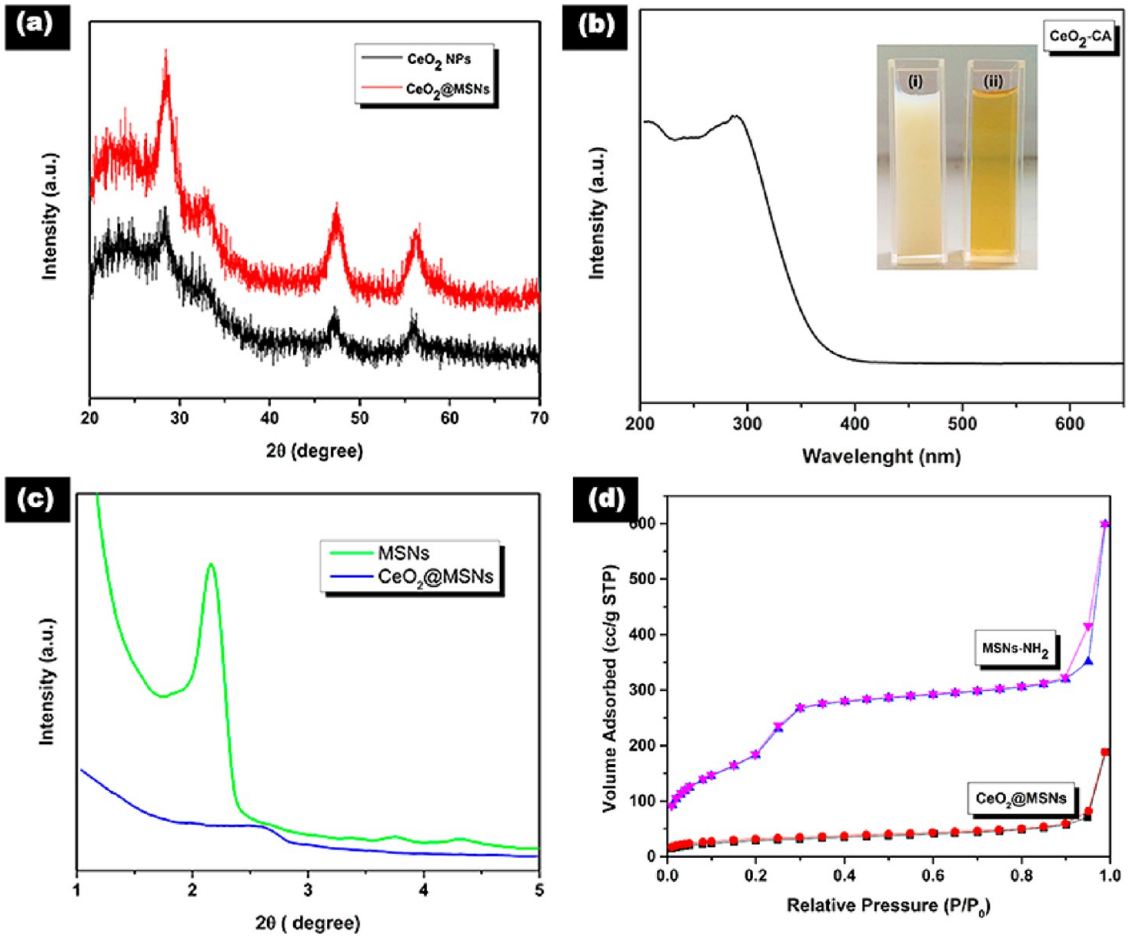

Figure 3. (a) High-angle XRD patterns of CeO_2 and CeO_2@MSNs. (b) Absorbance spectrum of citric acid capped CeO_2 NPs. Inset: Photographs demonstrate a marked difference in the quality of product before and after citric acid stabilization. (c) Low-angle X-ray diffraction (XRD) patterns of MSNs and CeO_2@MSNs. (d) Nitrogen adsorption−desorption isotherms for MSNs-NH_2 and CeO_2@MSNs samples.

Optical properties of colloidal solution of CeO_2 NPs was determined using UV−Vis spectroscopy; a prominent absorbance peak at about 290 nm was observed, which can be ascribed to the charge-transfer transitions from O 2p to Ce 4f, as can be seen in Figure 3b. Meanwhile, amine functionalized mesoporous silica nanoparticles (MSNs) were produced using a previously reported method. Empty channels of MSNs were then filled with different cargo molecules to perform proof-of-concept studies. Loading amounts of camptothecin (CPT) and rhodamin 6G (Rhd 6G) were measured through UV/vis spectroscopy. The relatively large quantities of both cargoes were loaded into nanochannels, encapsulated quantity of CPT and Rd 6G were determined to be 56 mg/g and 18 mg/g, respectively. Lastly, ultramsall CeO_2 nanolids were employed to seal drug loaded nanochannels of MSNs-NH_2 via EDC chemistry. Previously, bond dissociation has invariably been used in both polymer and MSNs based stimuli responsive drug release systems, but notably, no cleavable bonds are employed in this system to open the locked nanochannels. Only antioxidant susceptibility of CeO_2 NPs is exploited to unseal the drug encompassing channels for controlled drug release. Various analytical techniques were used to proof reducing agent mediated dissolution/etching phenomenon of CeO_2 NPs and subsequent gatekeeping concept.

Electron microscopy provides more credible information if ultrasmall nanoparticles are involved in blocking the drug loaded nanocarrier. SEM images displayed highly dispersed smooth surfaced MSNs nanospheres with a mean diameter of 100 nm (Figure 1). However, CeO_2 NPs immobilization transformed the plain exterior surface of MSNs into highly rough and dotted one. Large number of small and discrete dots can be seen on entire MSNs surface, thus suggesting the complete capping of drug loaded nanochannels (Figure 1b). In order to confirm CeO_2 NPs anchorage, EDX analysis was also done which revealed the presence of elemental cerium besides silicon and oxygen signals, as can be seen in Supporting Information Figure S4. Exposure of CeO_2@CPT@MSNs sample to reducing agents (vitamin C, glutathione) led to the appearance of extra aggregated product, in addition to spherical CeO_2@MSNs, as can be seen in Figure 1c, d. In order to gain further insight, TEM analysis was carried out, which furnished in depth information about the aggregated product. Initially, only drug loaded MSNs-NH_2 sample was examined, Figure 2c illustrates a well dispersed and nanosized MSNs with vivid two-dimensional ordered channels. The surface of these nanoparticles was smooth; however, a considerable change in MSNs surface was noticed after CeO_2 NPs immobilization. Large number of ultrasmall CeO_2 NPs covered the outer surface (Figure 2d).

TEM analysis similarly displayed large and aggregated cluster of CeO_2 besides drug encapsulated MSNs nanoparticles when CeO_2@CPT@MSNs were exposed to different concentrations of reducing agents. Figure 2e illustrates the effect of 1 mM ascorbic acid exposure on the morphology of CeO_2@CPT@

dx.doi.org/10.1021/am5055367 | ACS Appl. Mater. Interfaces 2014, 6, 19424−19433

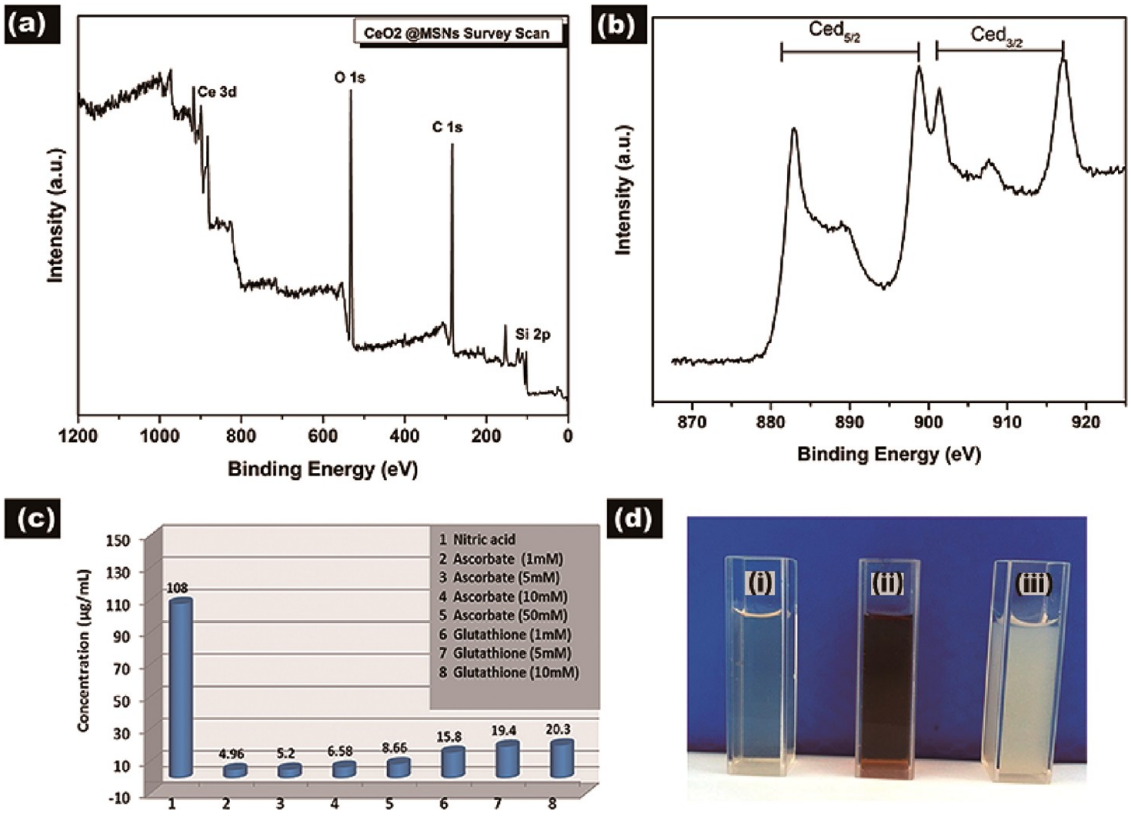

Figure 4. (a) XPS survey spectrum of CeO_2@MSNs (b) spectrum of Ce 3d, which reveals the coexistence of Ce^{3+} and Ce^{4+}. (c) Inductively coupled plasma (ICP) analysis after subjecting CeO_2@MSNs sample to nitric acid and different concentration of vitamin C and glutathione. (d) Photographs of citric acid stabilized CeO_2 NPs to demonstrate the interaction with biorelevant antioxidants, (i) CeO_2−CA, (ii) CeO_2 after vitamin C exposure. (iii) CeO_2 after glutathione treatment.

MSNs, nanocaps are detached from the surface of MSNs at biorelevant concentration, whereas, further increase in the strength of reducing agent lead to significant uncapping of drug loaded nanopores. Glutathione (intracellular reducing agent) was similarly tried as uncapping trigger, emergence of aggregated CeO_2 following the glutathione contact authenticated the opening of nanopores to release loaded drug molecules in a controlled fashion (Figure 2f). Upon careful inspection of clusters or aggregated product, it was found that aggregates were actually comprised of small CeO_2 NPs, crystalline nature and clear-cut boundaries of nanoparticles can be seen in high resolution images (Supporting Information Figure S5). A distinct change in particle size after dissolution/etching process was not detected in TEM analysis.

As far as MSNs capping goes, Figure 3c demonstrates a reduction in the intensity of characteristic MCM-41 (100) XRD peaks after drug loading and channels capping of MSNs-NH_2. Wide angle XRD also provided evidence regarding the immobilization of CeO_2 onto MSNs−NH_2 surface, identical XRD patterns as were noticed in case of mere CeO_2 NPs are also noticed but with weak intensities. Nitrogen adsorption surface analysis is consistently used to characterize porous nanomaterials. Following pores capping, BET surface area and pore volumes were decreased from 887 to 100 m^2/g and pore volume from 0.928 to 0.291 cm^3/g, respectively (Figure 3d and Supporting Information Figure S1).

XPS analysis also corroborated the successful anchorage of CeO_2 onto the surface of MSNs nanocarriers, Figure 4a shows survey spectrum of CeO_2 capped MSNs. Coexistence of cerium and silicon specific peaks (around 100 and 900 eV) verified the presence of CeO_2 nanoparticles. Similarly, higher resolution spectrum of cerium showed peaks of both Ce^{3+} and Ce^{4+} oxidation states, which are necessary for its redox activity. In order to quantify the immobilization and redox responsive dissolution of CeO_2 NPs, inductively coupled plasma mass spectrometry (ICP-MS) was carried out. CeO_2@MSNs sample was exposed to different concentrations of vitamin C and glutathione. Results indicated a significant amount of CeO_2 NPs immobilization (108 mg/g) onto MSNs surface. Subsequently, a specified amount of CeO_2@MSNs samples were introduced into both reducing agents solutions, approximately 5% of the total cerium was released when sample was subjected to 1 mM vitamin C. The release of cerium was amplified to ∼8% of the total cerium upon exposing the sample to 50 mM ascorbate solution. Likewise, glutathione exposure also resulted in the release of cerium ions according the concentration of glutathione. Relatively high amount of cerium was detected in case of GSH treatment, 10 mM GSH solution etched almost 18% CeO_2 NPs (Figure 4c). We monitored the release of Ce^{3+} for long time but we did not find any significant increase in cerium concentration. Figure 4d demonstrates the visible changes in the water stability and color of CeO_2 NPs solution after exposure to intracellular antioxidant molecules. First cuvette indicates a yellow, transparent and water dispersed CeO_2 NPs solution; however, GSH addition adversely affected its water stability and nanoparticles became aggregated, suggesting the reduction induced dissolution of outer stabilized layer of CeO_2 NPs and subsequent formation of disulfide linkages in glutathione molecules. On the other hand, introduction of vitamin C resulted in a stark color change in CeO_2 solution, yellow solution was instantly transformed into

dx.doi.org/10.1021/am5055367 | ACS Appl. Mater. Interfaces 2014, 6, 19424−19433

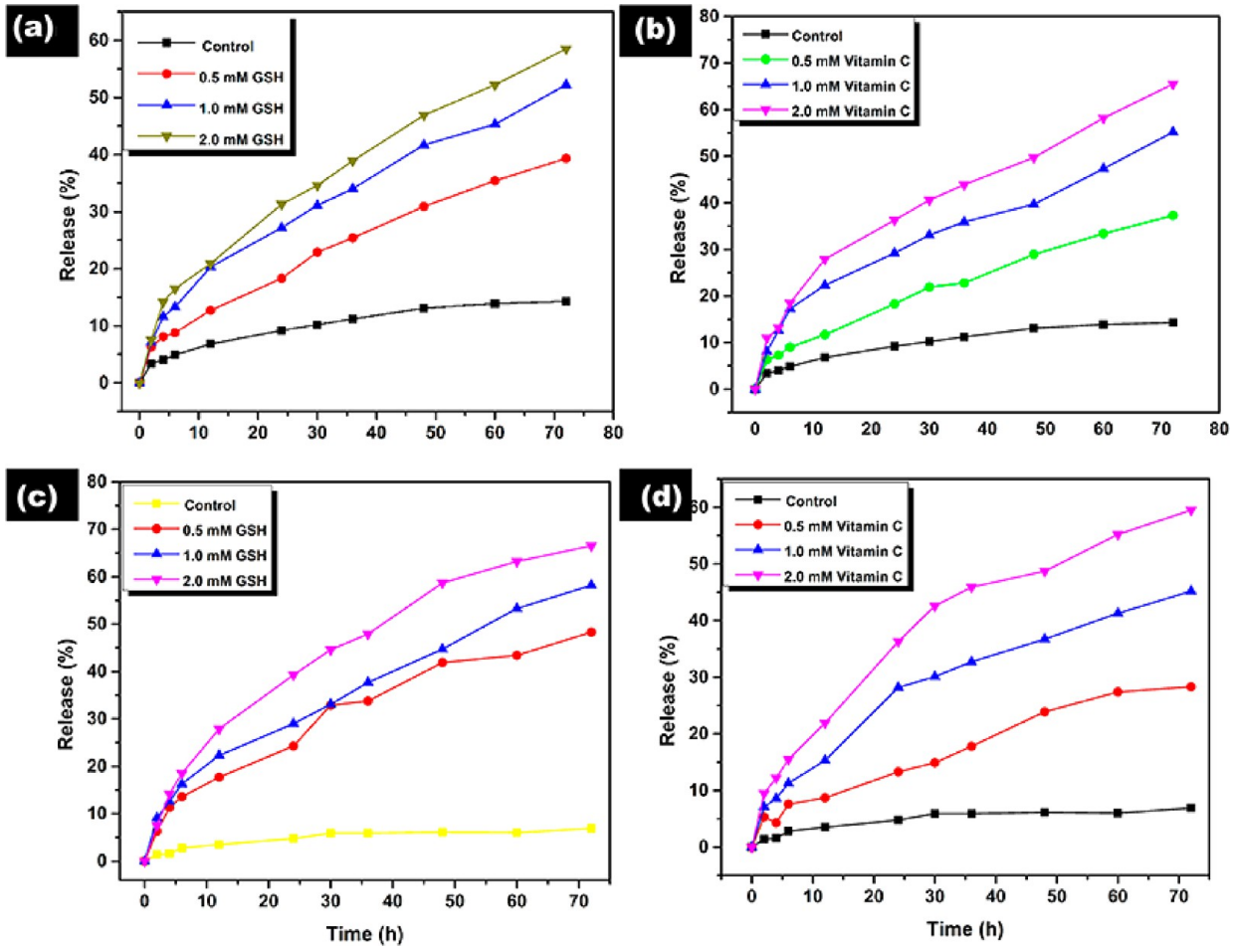

Figure 5. (a) Release profile of camptothecin from CeO_2@CPT@MSNs sample in the absence and presence of 0.5, 1.0, and 2.0 mM GSH. (b) Camptothecin release kinetics in control and in the presence of 0.5, 1.0, and 2.0 mM vitamin C. (c) Release profile of rhodamin 6G from CeO_2@Rhd@MSNs in the absence and presence of 0.5, 1.0, and 2.0 mM GSH. (d) Rhodamin 6G release kinetics in control and in the presence of 0.5, 1.0, and 2.0 mM vitamin C.

orange colored product; however, the stability of nanoparticles remained intact due to stabilizing nature of oxidized ascorbic acid (dehydroascorbic acid).

Antioxidant susceptibility of CeO_2 NPs and gatekeeping character of this system was investigated by studying the release kinetics of loaded cargo molecules (CPT and Rhd) from the pores of MSNs. When drug loaded and CeO_2 NPs capped MSNs were subjected to various concentrations of vitamin C and glutathione solution, antioxidant sensitive and controlled release of both cargoes was observed. Figure 5a demonstrates CPT release profile in the absence and presence of GSH (0.5−2 mM). In the absence of trigger, small amount of CPT was released (10%) from uncapped channels which suggested the effective capping of majority of CPT loaded nanopores. However, exposure of 0.5 mM GSH resulted in a ∼32% CPT release, which implied the onset of CeO_2 removal from the surface of MSNs. Significant quantity of CPT release was observed when concentration of GSH was amplified to 2 mM. Likewise, vitamin C was explored to induce the release of loaded CPT molecules (Figure 5b). When different concentrations of vitamin C were introduced into release system, a controlled release of CPT was detected, following almost the same release behavior as was noticed in GSH case, amount of drug release was enhanced with increasing concentration of vitamin C trigger. Vitamin C is an abundantly found nonenzymatic antioxidant, which plays a pivotal role in tackling oxidative stress, triggered by enhanced level of ROS.[43,44] Its antioxidant property is associated with its strong ability to donate electrons. In this study, ceria nanolids were reduced by vitamin C to remove from the surface of MSNs, which in turns opened the nanochannels of MSNs to allow controlled release of therapeutic molecules. To preclude any interaction between carrier and cargo, hydrophobic rhodamine 6G dye molecules were also loaded into channels of MSNs to prove gatekeeping concept. Dye loaded formulation was similarly subjected to various concentrations of glutathione and vitamin C. Figure 5(c, d) demonstrates the release profile of rhodamine 6G in the presence of antioxidants. These findings substantiated an antioxidant responsive and controlled release of cargo molecules. As mentioned above, reducing agents are generally used to cleave disulfide bonds for redox responsive release,[34] whereas in this study redox active CeO_2 NPs were not only used as nanolids but also served antioxidant sensitive entity for designing responsive drug release system.

To gauge the therapeutic potential of CeO_2 based MSNs nanoformulations, cell viability test was performed using a 3-(4,5-dimethylthiazol-2-yl)-2,5-diphenyltetrazolium bromide (MTT) assay. This assay monitored the mitochondrial dehydrogenase enzyme activity through dissociating the yellow MTT salt into purple colored formazan product. Pancreatic cancer cell line BxPc-3 was used as model, whereas different

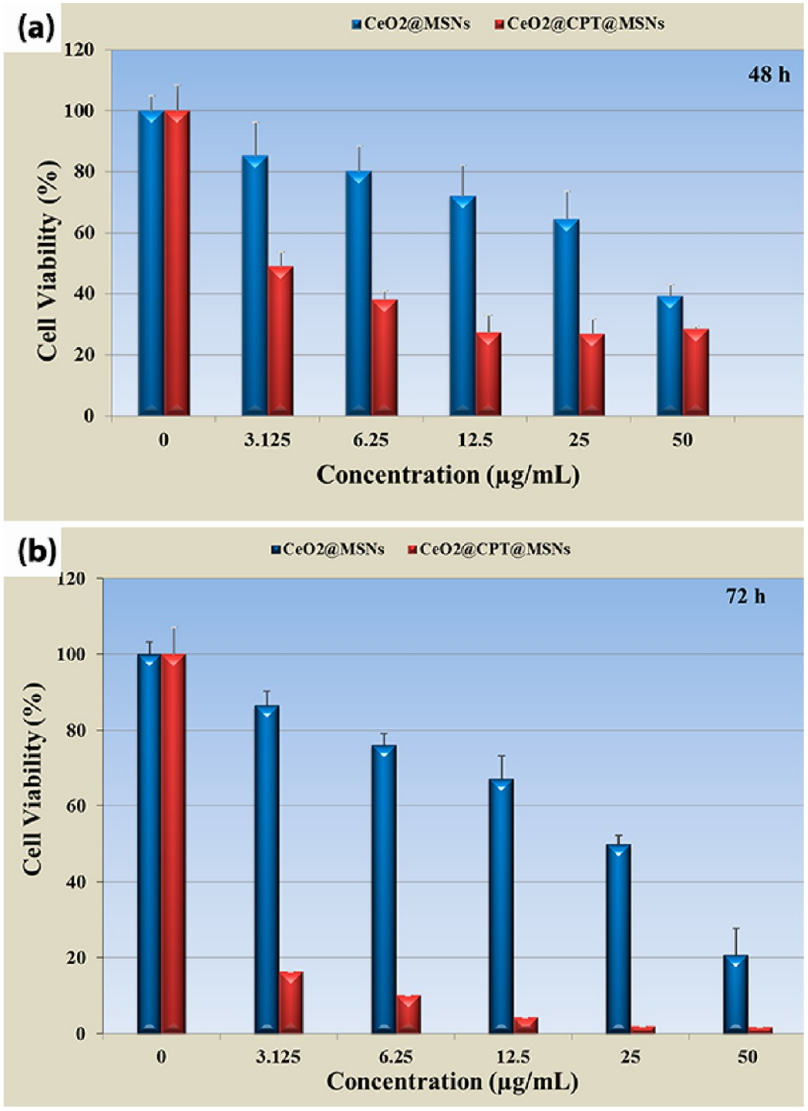

Figure 6. (a) In vitro viability of BxPC-3 cells in the presence of different concentrations of CeO_2@MSNs and CeO_2@CPT@MSNs nanoformulations, the incubation time was 48 h. (b) Cell viability of BxPC-3cells after 72 h incubation.

concentrations of MSNs nanoformulations (0.625−50 μg/mL) were incubation for 48 and 72 h. Biocompatibility of MSNs is well established, however we evaluated the cell viability of citrate stabilized CeO_2 NPs and results demonstrated high biocompatibility of nanoceria (Supporting Information Figure S6). No cytotoxic effects were observed at as high concentration as 500 μg/mL. Figure 6a shows the percentage of viable cells after 48 h incubation of CeO_2@MSNs nanoformulation, a slight decrease in cell viability was observed following cell exposure. This slight toxicity of nanocomposite can be ascribed to enhanced cellular uptake of CeO_2@MSNs. It has been previously reported that negatively charged citrate stabilized CeO_2 exhibits low intracellular uptake, but after immobilization of CeO_2 on MSN surface, the ζ-potential value is reduced from −35 to −18, which enhances the possibility of cellular uptake. Camptothecin loaded nanoformulation (CeO_2@CPT@MSNs) exhibited substantially high cell growth inhibiting capacity, inactivating 60% of the cells at just 6 μg/mL concentration. Further increase in the drug loaded sample resulted in an enhanced killing capability, as can be seen in Figure 6a. Compared to 48 h incubation, 72 h incubations of CeO_2@CPT@MSNs nanoformulation proved exceptionally lethal, 85% cells were killed at as low as 3 μg/mL due to controlled release behavior (Figure 6b). Therapeutic efficacy of CeO_2@CPT@MSNs was only possible when clogged nanopores of MSNs were opened in intracellular environment; these excellent cytotoxic results of MTT assay strongly suggest the uncapping of MSNs in highly reducing cellular environment.

Intracellular uptake, antioxidant-activated dissolution of CeO_2 and subsequent release of encapsulated cargo molecules was monitored in real time by confocal microscopy. Definite amount of rhodamin 6G and camptothecin loaded MSNs formulations (50 μg/mL) were incubated with BxPc-3 cells for 6 hours. Nucleus of cells was first stained with Hoechst dye, blue fluorescent nucleus of BxPc-3 cells can be seen in Figure 7(a, d, g). Following CeO_2@CPT@MSNs incubation, CLSM images implied the cellular uptake of nanoparticles in the form of more intense and dotted blue luminescence in the cytoplasmic and nuclear regions, because MSNs loaded CPT also fluoresces blue light when irradiated under 404 nm laser.

As our CPT loaded MSNs sample was capped with CeO_2 NPs, however, the appearance of such dotted and more intense blue luminescence in cellular compartments implied the release of

dx.doi.org/10.1021/am5055367 | ACS Appl. Mater. Interfaces 2014, 6, 19424−19433

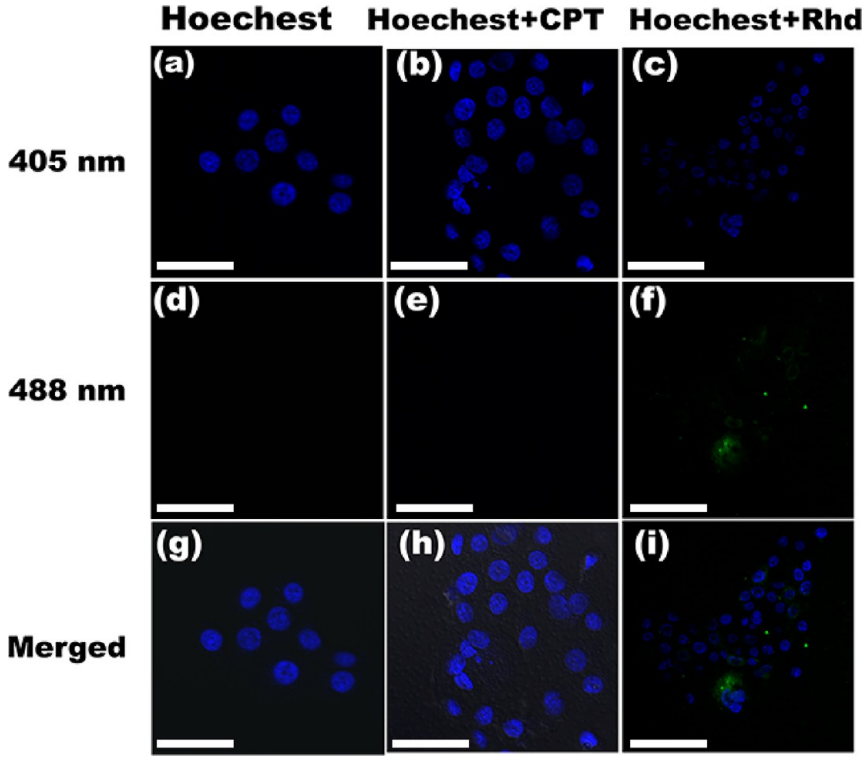

Figure 7. CLSM micrographs of BxPC-3 cells after 6 h incubation with CeO_2@CPT@MSNs and CeO_2@Rhd @MSNs nanoformulations (50 μg/mL). Column 1 illustrates hoechest pretreated cells and images a and d are obtained by irradiating cells with 405 and 488 nm lasers, whereas image g is the overlay image of a and d. Column 2 indicates neclear-stained and CeO_2@CPT@MSNs treated cells, image b and e are obtained by irradiating cells with 405 and 488 nm lasers, whereas image h is the overlay images of b and e. Column 3 indicates neclear-stained and CeO_2@Rhd@MSNs treated cells, image c and f are obtained by irradiating cells with 405 and 488 nm lasers, whereas image i is the overlay image of c and f. Length of scale bar = 50 μM.

loaded CPT molecules. All above-mentioned characterization techniques have convincingly proved the redox sensitive behavior of CeO_2 NPs, therefore, highly reducing intracellular environment of cells possibly caused CeO_2 etching-accompanied release of luminescent anticancer drug molecules. Due to blue luminescence of both species, dissimilar colored rhodamin 6G loaded samples (CeO_2@Rhd@MSNs) was also examined to achieve better contrast (Figure 7(f, i)). In case of CeO_2@Rhd@MSNs incubation, besides blue-stained nucleus, green fluorescence in the cytoplasmic regions is also observed, thus representing the uncapping of MSNs to sustainably release loaded rhodamin 6G molecules. Taken together, the release of camptothecin and rhodamin 6G molecules suggested a responsive and controlled release of cargo as noticed in drug release profile.

3. CONCLUSIONS

In conclusion, the current study investigated the interaction of manmade regenerative antioxidant nanoparticles (CeO_2 NPs) with biological antioxidants. It was demonstrated that stable CeO_2 NPs were highly susceptible to vitamin C and glutathione. Exposure of biorelavent antioxidants led to dissolution-accompanied aggregation of CeO_2 NPs. We subsequently exploited the redox sensitive behavior of nanoceria as biological trigger to design mesoporous silica based responsive drug delivery system. Proof of concept studies and in vitro cell experiments vividly demonstrated that the dissolution of one therapeutic nanoparticle (CeO_2) unleashed another therapeutic entity from the nanoreservoir of mesoporous silica to cause excellent anticancer efficiency. More importantly, this report unravels a key interaction between nanoceria and biologically significant components.

■ ASSOCIATED CONTENT

Ⓢ Supporting Information

Materials, characterization, infrared spectrum, XPS survey scan, ζ-potential, HRTEM micrograph, and cell viability data is provided. This material is available free of charge via the Internet at http://pubs.acs.org.

■ AUTHOR INFORMATION

Corresponding Author

*E-mail: zhugs@jlu.edu.cn.

Notes

The authors declare no competing financial interest.

■ ACKNOWLEDGMENTS

We are grateful to the financial support from National Basic Research Program of China (973 Program, grant nos. 2012CB821700), Major International (Regional) Joint Research Project of NSFC (grant nos. 21120102034), and NSFC (grant nos. 20831002).

■ REFERENCES

(1) Coussens, L. M.; Werb, Z. Inflammation and Cancer. *Nature* **2002**, *420*, 860−867.

(2) Hole, P. S.; Darley, R. L.; Tonks, A. Do Reactive Oxygen Species Play a Role in Myeloid Leukemias? *Blood* **2011**, *117*, 5816−5826.

(3) Hybertson, B. M.; Gao, B.; Bose, S. K.; McCord, J. M. Oxidative Stress in Health and Disease: The Therapeutic Potential of Nrf2 Activation. *J. Mol. Aspects. Med.* **2011**, *32*, 234−246.

(4) Valko, M.; Rhodes, C. J.; Moncol, J.; Izakovic, M.; Mazur, M. Free Radicals, Metals and Antioxidants in Oxidative Stress-Induced Cancer. *Chem. Biol. Interact.* **2006**, *160*, 1−40.
(5) Ames, B. N.; Shigenaga, M. K.; Hagen, T. M. Oxidants, Antioxidants, and the Degenerative Diseases of Aging. *Proc. Natl. Acad. Sci. U. S. A.* **1993**, *90*, 7915−7922.
(6) Chaudière, J.; Ferrari-Iliou, R. Intracellular Antioxidants: from Chemical to Biochemical Mechanisms. *Food Chem. Toxicol.* **1999**, *37*, 949−962.
(7) Bitner, B. R.; Marcano, D. C.; Berlin, J. M.; Fabian, R. H.; Cherian, L.; Culver, J. C.; Dickinson, M. E.; Robertson, C. S.; Pautler, R. G.; Kent, T. A.; Tour, J. M. Antioxidant Carbon Particles Improve Cerebrovascular Dysfunction Following Traumatic Brain Injury. *ACS Nano* **2012**, *6*, 8007−8014.
(8) Lucente-Schultz, R. M.; Moore, V. C.; Leonard, A. D.; Price, B. K.; Kosynkin, D. V.; Lu, M.; Partha, R.; Conyers, J. L.; Tour, J. M. Antioxidant Single-Walled Carbon Nanotubes. *J. Am. Chem. Soc.* **2009**, *131*, 3934−3941.
(9) Lee, S. S.; Song, W.; Cho, M.; Puppala, H. L.; Nguyen, P.; Zhu, H.; Segatori, L.; Colvin, V. L. Antioxidant Properties of Cerium Oxide Nanocrystals as a Function of Nanocrystal Diameter and Surface Coating. *ACS Nano* **2013**, *7*, 9693−9703.
(10) Karakoti, A.; Singh, S.; Dowding, J. M.; Seal, S.; Self, W. T. Redox-Active Radical Scavenging Nanomaterials. *Chem.Soc.Rev.* **2010**, *39*, 4422−4432.
(11) Chen, J.; Patil, S.; Seal, S.; McGinnis, J. F. Rare Earth Nanoparticles Prevent Retinal Degeneration Induced by Intracellular Peroxides. *Nat. Nanotechnol.* **2006**, *1*, 142−150.
(12) Hirst, S. M.; Karakoti, A. S.; Tyler, R. D.; Sriranganathan, N.; Seal, S.; Reilly, C. M. Anti-Inflammatory Properties of Cerium Oxide Nanoparticles. *Small* **2009**, *5*, 2848−2856.
(13) Karakoti, A. S.; Singh, S.; Kumar, A.; Malinska, M.; Kuchibhatla, S. V. N. T.; Wozniak, K.; Self, W. T.; Seal, S. Pegylated Nanoceria as Radical Scavenger with Tunable Redox Chemistry. *J. Am. Chem. Soc.* **2009**, *131*, 14144−14145.
(14) Pagliari, F.; Mandoli, C.; Forte, G.; Magnani, E.; Pagliari, S.; Nardone, G.; Licoccia, S.; Minieri, M.; Di Nardo, P.; Traversa, E. Cerium Oxide Nanoparticles Protect Cardiac Progenitor Cells from Oxidative Stress. *ACS Nano* **2012**, *6*, 3767−3775.
(15) Perez, J. M.; Asati, A.; Nath, S.; Kaittanis, C. Synthesis of Biocompatible Dextran-Coated Nanoceria with pH-Dependent Antioxidant Properties. *Small* **2008**, *4*, 552−556.
(16) Kim, C. K.; Kim, T.; Choi, I.-Y.; Soh, M.; Kim, D.; Kim, Y.-J.; Jang, H.; Yang, H.-S.; Kim, J. Y.; Park, H.-K.; Park, S. P.; Park, S.; Yu, T.; Yoon, B.-W.; Lee, S.-H.; Hyeon, T. Ceria Nanoparticles that can Protect Against Ischemic Stroke. *Angew. Chem., Int. Ed.* **2012**, *51*, 11039−11043.
(17) Heckert, E. G.; Karakoti, A. S.; Seal, S.; Self, W. T. The Role Of Cerium Redox State in the SOD Mimetic Activity of Nanoceria. *Biomaterials* **2008**, *29*, 2705−2709.
(18) Pirmohamed, T.; Dowding, J. M.; Singh, S.; Wasserman, B.; Heckert, E.; Karakoti, A. S.; King, J. E. S.; Seal, S.; Self, W. T. Nanoceria Exhibit Redox State-dependent Catalase Mimetic Activity. *Chem. Commun.* **2010**, *46*, 2736−2738.
(19) Celardo, I.; De Nicola, M.; Mandoli, C.; Pedersen, J. Z.; Traversa, E.; Ghibelli, L. Ce^{3+} Ions Determine Redox-Dependent Anti-Apoptotic Effect of Cerium Oxide Nanoparticles. *ACS Nano* **2011**, *5*, 4537−4549.
(20) Tarnuzzer, R. W.; Colon, J.; Patil, S.; Seal, S. Vacancy Engineered Ceria Nanostructures for Protection from Radiation-Induced Cellular Damage. *Nano Lett.* **2005**, *5*, 2573−2577.
(21) Kuchibhatla, S. V. N. T.; Karakoti, A. S.; Baer, D. R.; Samudrala, S.; Engelhard, M. H.; Amonette, J. E.; Thevuthasan, S.; Seal, S. Influence of Aging and Environment on Nanoparticle Chemistry: Implication to Confinement Effects in Nanoceria. *J. Phys. Chem. C* **2012**, *116*, 14108−14114.
(22) Hoecke, K. V.; Quik, J. T. K.; Mankiewicz-Boczek, J.; Schamphelaere, K. A. C. D.; Elsaesser, A.; Meeren, P. V. d.; Barnes, C.; McKerr, G.; Howard, C. V.; Meent, D. V. D.; Rydzyński, K.; Dawson, K. A.; Salvati, A.; Lesniak, A.; Lynch, I.; Silversmit, G.; Samber, B. D.; Vincze, L.; Janssen, C. R. Fate and Effects of CeO_2 Nanoparticles in Aquatic Ecotoxicity Tests. *Environ. Sci. Technol.* **2009**, *43*, 4537−4546.
(23) Ma, C.; Chhikara, S.; Xing, B.; Musante, C.; White, J. C.; Dhankher, O. P. Physiological and Molecular Response of *Arabidopsis thaliana* (L.) to Nanoparticle Cerium and Indium Oxide Exposure. *ACS Sustainable Chem. Eng.* **2013**, *1*, 768−778.
(24) Zhang, P.; Ma, Y.; Zhang, Z.; He, X.; Zhang, J.; Guo, Z.; Tai, R.; Zhao, Y.; Chai, Z. Biotransformation of Ceria Nanoparticles in Cucumber Plants. *ACS Nano* **2012**, *6*, 9943−9950.
(25) Cornelis, G.; Ryan, B.; McLaughlin, M. J.; Kirby, J. K.; Beak, D.; Chittleborough, D. Solubility and Batch Retention of CeO_2 Nanoparticles in Soils. *Environ. Sci. Technol.* **2011**, *45*, 2777−2782.
(26) Rojas, S.; Gispert, J. D.; Abad, S.; Buaki-Sogo, M.; Victor, V. M.; Garcia, H.; Herance, J. R. In Vivo Biodistribution of Amino-Functionalized Ceria Nanoparticles in Rats Using Positron Emission Tomography. *Mol. Pharm.* **2012**, *9*, 3543−3550.
(27) Singh, S.; Dosani, T.; Karakoti, A. S.; Kumar, A.; Seal, S.; Self, W. T. A Phosphate-Dependent Shift in Redox State of Cerium Oxide Nanoparticles and Its Effects on Catalytic Properties. *Biomaterials* **2011**, *32*, 6745−6753.
(28) Mura, S.; Nicolas, J.; Couvreur, P. Stimuli-Responsive Nanocarriers for Drug Delivery. *Nat. Mater.* **2013**, *12*, 991−1003.
(29) Gao, W.; Chan, J. M.; Farokhzad, O. C. pH-Responsive Nanoparticles for Drug Delivery. *Mol. Pharmaceutics* **2010**, *7*, 1913−1920.
(30) Davis, M. E.; Chen, Z.; Shin, D. M. Nanoparticle Therapeutics: An Emerging Treatment Modality for Cancer. *Nat. Rev. Drug Discovery* **2008**, *7*, 771−782.
(31) Zhao, F.; Shen, G.; Chen, C.; Xing, R.; Zou, Q.; Ma, G.; Yan, X. Nanoengineering of Stimuli-Responsive Protein-Based Biomimetic Protocells as Versatile Drug Delivery Tools. *Chem.—Eur. J.* **2014**, *20*, 6880−6887.
(32) Yang, Y.; Li, J. Lipid, Protein, and Poly(NIPAM) Coated Mesoporous Silica Nanoparticles for Biomedical Applications. *Adv. Colloid Interface Sci.* **2014**, *207*, 155−163.
(33) Yan, X.; Li, J.; Möhwald, H. Templating Assembly of Multifunctional Hybrid Colloidal Spheres. *Adv. Mater.* **2012**, *24*, 2663−2667.
(34) Vivero-Escoto, J. L.; Slowing, I. I.; Trewyn, B. G.; Lin, V. S. Y. Mesoporous Silica Nanoparticles for Intracellular Controlled Drug Delivery. *Small* **2010**, *6*, 1952−1967.
(35) Wu, S.-H.; Hung, Y.; Mou, C.-Y. Mesoporous Silica Nanoparticles as Nanocarriers. *Chem. Commun.* **2011**, *47*, 9972−9985.
(36) Muhammad, F.; Guo, M.; Qi, W.; Sun, F.; Wang, A.; Guo, Y.; Zhu, G. pH-Triggered Controlled Drug Release from Mesoporous Silica Nanoparticles via Intracelluar Dissolution of ZnO Nanolids. *J. Am. Chem. Soc.* **2011**, *133*, 8778−8781.
(37) Luo, Z.; Cai, K.; Hu, Y.; Zhao, L.; Liu, P.; Duan, L.; Yang, W. Mesoporous Silica Nanoparticles End-Capped with Collagen: Redox-Responsive Nanoreservoirs for Targeted Drug Delivery. *Angew. Chem., Int. Ed.* **2011**, *50*, 640−643.
(38) Napoli, A.; Valentini, M.; Tirelli, N.; Muller, M.; Hubbell, J. A. Oxidation-Responsive PolymericVesicles. *Nat. Mater.* **2004**, *3*, 183−189.
(39) Mal, N. K.; Fujiwara, M.; Tanaka, Y. Photocontrolled Reversible Release of Guest Molecules from Coumarin-Modified Mesoporous Silica. *Nature* **2003**, *421*, 350−353.
(40) Schlossbauer, A.; Kecht, J.; Bein, T. Biotin−Avidin as a Protease-Responsive Cap System for Controlled Guest Release from Colloidal Mesoporous Silica. *Angew. Chem., Int. Ed.* **2009**, *48*, 3092−3095.
(41) Krishnan, A.; Sreeremya, T. S.; Murray, E.; Ghosh, S. One-Pot Synthesis of Ultra-Small Cerium Oxide Nanodots Exhibiting Multi-Colored Fluorescence. *J Colloid Interf. Sci.* **2013**, *389*, 16−22.
(42) Sreeremya, T. S.; Thulasi, K. M.; Krishnan, A.; Ghosh, S. A Novel Aqueous Route to Fabricate Ultrasmall Monodisperse Lipophilic Cerium Oxide Nanoparticles. *Ind. Eng. Chem. Res.* **2011**, *51*, 318−326.
(43) Bendich, A.; Machlin, L. J.; Scandurra, O.; Burton, G. W.; Wayner, D. D. M.The Antioxidant Role of Vitamin C. *Adv. Free Radic. Biol. Med.* **1986**, *2*, 419−444.

(44) Montecinos, V.; Guzmán, P.; Barra, V.; Villagrán, M.; Muñoz-Montesino, C.; Sotomayor, K.; Escobar, E.; Godoy, A.; Mardones, L.; Sotomayor, P.; Guzmán, C.; Vásquez, O.; Gallardo, V.; van Zundert, B.; Bono, M. R.; Oñate, S. A.; Bustamante, M.; Cárcamo, J. G.; Rivas, C. I.; Vera, J. C. Vitamin C Is an Essential Antioxidant that Enhances Survival of Oxidatively Stressed Human Vascular Endothelial Cells in the Presence of a Vast Molar Excess of Glutathione. *J. Biol. Chem.* **2007**, *282*, 15506−15515.